

Photocatalytic degradation of RhB, MG, MB, Roz.B, 3-BL and CI-50 by PW_{12} -APTES@MCF as nanosized mesoporous photocatalyst

Razieh Fazaeli · Hamid Aliyan · Shahram Tangestaninejad · Somaieh Parishani Foroushani

Received: 25 July 2013 / Accepted: 22 February 2014 / Published online: 12 March 2014
© Iranian Chemical Society 2014

Abstract Surface of mesocellular silica foam (MCF) was modified by grafting 3-aminopropyltriethoxysilane (APTES) to have the positive charge, and thus, to provide sites for the immobilization of $H_3PW_{12}O_{40}$ (PW_{12}). This modified-nanosized mesoporous silica (PW_{12} -APTES@MCF) was characterized by FTIR, XRD, BET and TEM. The photoefficiency of this nanosized mesoporous toward photodegradation of six dye solutions [rhodamine B, malachite green, methylene blue, rose bengal, solophenyl red (3-BL), yellow direct 50 (CI-50)] was investigated in a photocatalytic reactor using UV lamp as a light source. The effect of various experimental parameters on the degradation performance of the process was evaluated by examining catalyst dosage, initial dye concentration and pH of the dye solution in the presence of PW_{12} -APTES@MCF. The photocatalytic behaviors of the PW_{12} -APTES@MCF were also compared with two mesoporous silica-supported PW_{12} -APTES@SBA-15 and PW_{12} -APTES@KIT-6. It indicated that the PW_{12} -APTES@MCF had the highest photocatalytic efficiency among three mesoporous silica-supported PW_{12} -APTES. These photocatalysts can be reused several times although they get less active.

Keywords Mesocellular silica foam (MCF) · Heterogeneous photocatalysis · Polyoxotungstate

Introduction

Dye pollutants from the textile industry are an important source of environmental contamination. It is estimated that 1–15 % of the dye is lost during dyeing processes and is released in wastewaters [1]. The release of these colored wastewaters in the eco system is a dramatic source of esthetic pollution, eutrophication and perturbations in aquatic life [2]. A variety of physical, chemical and biological methods are presently available for treatment of textile wastewater. Biological treatment is a proven technology and is cost effective. However, it has been reported that the majority of dyes are only adsorbed on the sludge and are not degraded [3]. Physical methods such as ion exchange, adsorption, air stripping, etc., are also ineffective on pollutants which are not readily adsorbable or volatile, and have the further disadvantage that they simply transfer the pollutants to another phase rather than destroying them. This leads to search for highly effective method to degrade the dyes into environmentally compatible products [4–7].

Ordered mesoporous silicas represent a class of materials that can be used as adsorbents [8]. The most important characteristics of the mesoporous silicas are the large surface area, high mesopore volume, and narrow pore size distribution in the range of mesopores. However, many applications (such as adsorption, ion exchange, catalysis and sensing) require these silica-based materials to have specific attributes such as binding sites, stereochemical configuration, charge density and acidity [9]. Functionalization of the silica surface with organic groups is very

R. Fazaeli (✉) · S. Parishani Foroushani
Department of Chemistry, Shahreza Branch,
Islamic Azad University, 86145-311 Isfahan, Iran
e-mail: fazaelirazieh@yahoo.com; fazaeli@iaush.ac.ir

H. Aliyan
Department of Chemistry, Mobarakeh Branch,
Islamic Azad University, 84815-119 Isfahan, Iran

S. Tangestaninejad
Department of Chemistry, Isfahan University,
81746-73441 Isfahan, Iran

important and can be achieved via post synthesis grafting or direct co-condensation synthesis routes [10, 11].

The photochemical behavior of polyoxometalates (POMs) has been studied extensively in homogeneous systems, and it indicates that the photo-oxidation efficiency of POMs is comparable to that of the semiconductor TiO_2 [12–19]. The major drawback to the practical applications of POM photocatalytic systems is the high water solubility of POMs, which impedes ready recovery and reuse of the photocatalysts [20]. Otherwise, the active sites on the surface of the catalyst are small because of the low-specific surface areas of solid POMs (ca. $5 \text{ m}^2/\text{g}$). Therefore, two main methods for the preparation of insoluble POMs are considered, i.e., precipitation with a counter cation such as Cs^+ to form $\text{Cs}_3\text{PW}_{12}\text{O}_{40}$ colloidal [21], and immobilization of POMs into the solid matrix [22]. The latter is more and more interesting, because the support makes POMs easily handled and recycled [23–26].

In continuation of our work on the catalytic properties of heteropoly acids (HPAs) [27–29], herein, we investigate on the characteristics of the $\text{H}_3\text{PW}_{12}\text{O}_{40}$ catalyst immobilized on the 3-aminopropyltriethoxysilane (APTES)-modified mesocellular silica foam MCF (donated as $\text{PW}_{12}\text{-APTES@MCF}$, hereafter). The photocatalytic activities of this nanoporous composite have been evaluated using three commercial cationic dyes [Rhodamine B (RhB), Malachite green (MG), Methylene blue (MB)] and three commercial anionic dyes [Rose Bengal (Roz.B), Solophenyl red (3-BL or C.I. Direct 80), Yellow direct 50 (CI-50)] as model pollutants. Choosing these dyes as pollutant molecules is because of their importance as dyes in textile industry and other various applications. These dyes are toxic and carcinogenic, and hence a number of researchers have made attempts for the degradation of these dyes [30–32]. The influences of experimental parameters were studied to achieve to a better degradation efficiency of dyes. The color removal of dye solutions without catalyst was studied in all experiments. The rate constant, k , was calculated from the slopes of the straight-line portion of the plots of $\ln(C/C^0)$ vs. time. To our knowledge, this is first study of $\text{PW}_{12}\text{-APTES@KIT-6}$ toward RhB, MG, MB, Roz.B, 3-BL, CI-50 photodegradations.

Experimental

All chemicals and reagents were purchased from Sigma-Aldrich. Chemical structures, molecular weight (g/mol) and λ_{max} (nm) of the six used dyes are shown in Table 1. Infrared spectra ($400\text{--}4,000 \text{ cm}^{-1}$) were recorded from KBr pellets on a PerkinElmer Spectrum 65 spectrometer. The X-ray powdered diffraction patterns were performed on a Bruker-D8ADVANCE with automatic control. The

patterns were run with monochromatic $\text{Cu K}\alpha$ (1.5406 \AA) radiation with a scan rate of 2° min^{-1} . Nitrogen adsorption measurements were performed at $-196 \text{ }^\circ\text{C}$ using an ASAP 2010 M surface analyzer, and the pretreatment temperature was $180 \text{ }^\circ\text{C}$. Transmission electron micrographs (TEM) were obtained on a Joel JEM 2010 scan-transmission electron microscope. The sample for the TEM measurement was suspended in ethanol and supported on a carbon-coated copper grid. The UV light source was a Hg lamp (75 W). The absorption spectra were registered on a double beam spectrophotometer (Carry 100 Scan) in suprasil quartz cells of 1-cm optical path length, and the absorbance of samples was measured in the wavelength range of 190–900 nm. In order to remove photocatalyst particles before analysis, the suspensions were centrifuged with “type-H-11n” and 3,500 rpm for 5 min. The influence of pH on the absorption was studied by adding HCl or NaOH solutions to the suspensions. Total organic carbon (TOC) measurements were carried out by TOC analyzer of Shimadzu TOC-VCSN (Japan).

Synthesis of mesoporous MCF

The mesoporous MCF support was prepared as described previously [33] using a the Pluronic P123 triblock copolymer ($\text{EO}_{20}\text{PO}_{70}\text{EO}_{20}$) surfactant with 1,3,5-trimethylbenzene (TMB) as the organic swelling agent. A solution of P123:TMB:1.6 mol/L HCl:tetraethoxysilane (TEOS) = 2:1.5:75:4.25 (mass ratio) was prepared at $40 \text{ }^\circ\text{C}$. After 24 h at $40 \text{ }^\circ\text{C}$, the milky reaction mixture was transferred to an autoclave and crystallized at $100 \text{ }^\circ\text{C}$ for 48 h. The solid product was filtered, washed, dried at $90 \text{ }^\circ\text{C}$, and eventually calcined at $600 \text{ }^\circ\text{C}$ for 5 h in air to remove the template.

Surface modification of MCF and immobilization of $\text{H}_3\text{PW}_{12}\text{O}_{40}$

Scheme 1 shows the procedures for the surface modification of MCF and the subsequent immobilization of $\text{H}_3\text{PW}_{12}\text{O}_{40}$ (PW_{12}) on the APTES@MCF. Surface modification of MCF was done by a grafting method [34].

To a suspension of 10 g of calcined MCF in 50 mL dry toluene, 2.68 g of 3-aminopropyltriethoxysilane was added slowly and heated to reflux with continuous stirring for 8 h under nitrogen atmospheres. The powdery sample containing amino groups was filtered, washed with acetone and then soxhlet extracted using a solution mixture of diethyl ether and dichloromethane (1:1) for 24 h and dried under vacuum. It was finally calcined at $180 \text{ }^\circ\text{C}$ for 2 h to yield the APTES@MCF. Immobilization of PW_{12} on the APTES@MCF was achieved as following. APTES@MCF (1.0 g) was added into the acetonitrile solution (5 mL)

Table 1 The structures, molecular weight and λ_{\max} of the used commercial dyes

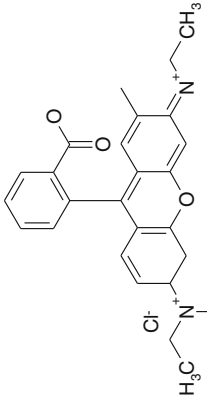
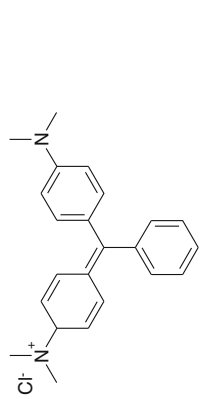
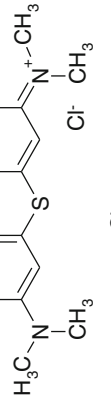
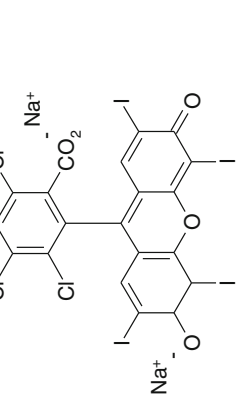
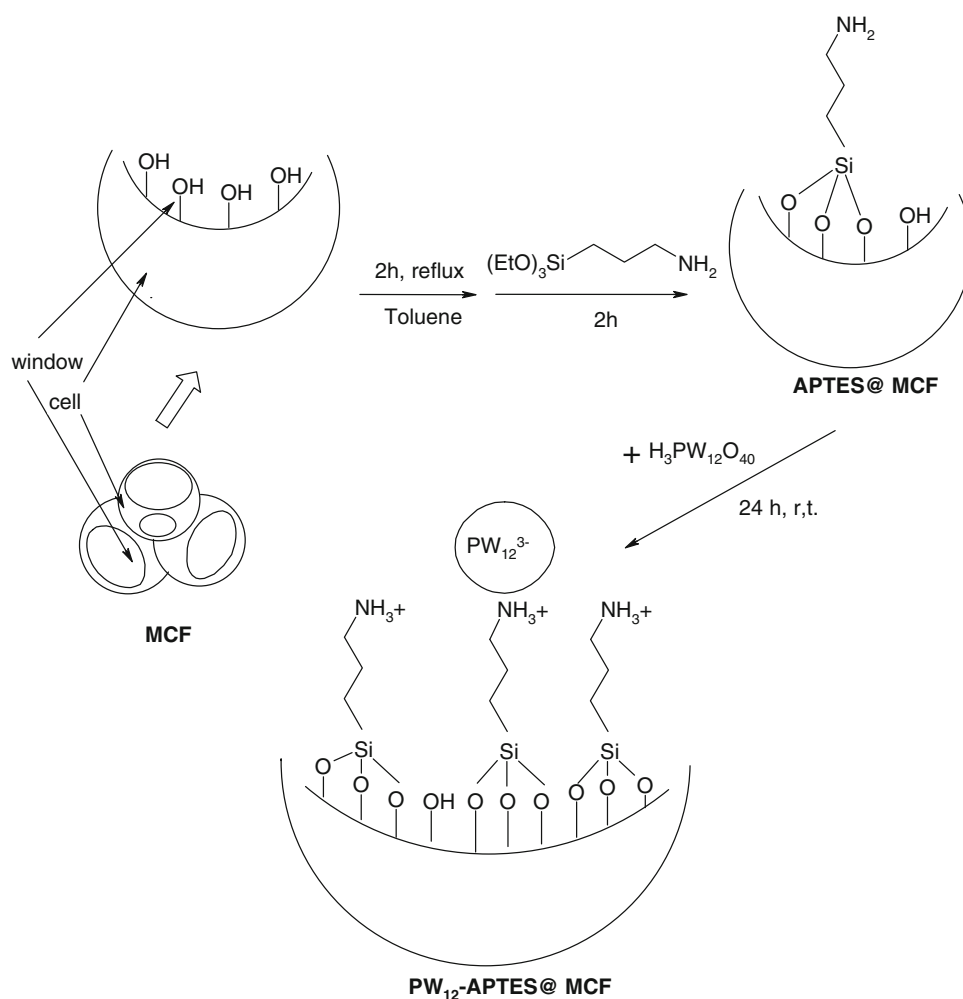
Dye	Structural formula	Molecular weight (g/mol)	λ_{\max} (nm)
Rhodamine B (RhB)		479.0	546.0
Malachite green (MG)		364.9	621.0
Methylene blue (M.B)		319.9	661.0
Rose bengal (Roz.B)		1,017	545.0

Table 1 continued

Dye	Structural formula	Molecular weight (g/mol)	λ_{\max} (nm)
Solophenyl red (3-BL)		1,373	530.0
Yellow direct 50 (CI-50)		956.8	390.0

Scheme 1 The procedures for the surface modification of MCF and the subsequent immobilization of PW_{12} on APTES@MCF



containing 0.5 g of PW_{12} with vigorous stirring at room temperature, and the resulting solution was maintained at room temperature for 24 h. The solid product was filtered, and then it was dried overnight at 80 °C to yield the PW_{12} -APTES@MCF [34].

Photocatalytic activity

Photodegradation experiments were performed with a photocatalytic reactor system. The bench-scale system is a cylindrical Pyrex-glass cell with 1.0-L capacity, 10-cm inside diameter and 15-cm height. Irradiation experiments were performed using medium pressure Hg lamp (75 W), then it was placed in a 5-cm diameter quartz tube with one end tightly sealed by a Teflon stopper. The inner tube containing the lamp was placed directly into the outer Pyrex tube so that the solution was between the two tubes and directly exposed to the UV emanating from the quartz tube. The lamp and the tube were then immersed in the photoreactor cell with a light path of 3.0 cm. A magnetic stirrer was used continuously to guarantee good mixing of the solution. Generally, HCl (1 M) and NaOH (1 M) were used to adjust

the pH value in the beginning of all experiments including the effect of pH study. The decolorization of the six commercial dyes [Rhodamine B (RhB), Malachite green (MG), Methylene blue (MB), Rose bengal (Roz.B), Solophenyl red (3-BL), Yellow direct 50 (CI-50)] were analyzed by UV–Vis spectrophotometer (Cary 100 Scan). The decolorization was determined at the wavelength of maximum absorption of each dye. In the investigation of pH, due to shift in the λ_{max} value, new λ_{max} was determined by scanning the samples at a range of 190–900 nm. Decolorization efficiency was determined using absorbance of solutions before and after photodecolorization experiments. To determine the surface adsorption amount, control experiments in the dark condition were carried out in parallel in each case in the presence of catalyst during the decolorization of the mentioned six dyes. The decolorization efficiency of the dye was determined by the following equation (Eq. 1):

$$\text{Decolorization efficiency (\%)} = \frac{C_0 - C}{C_0} \times 100 \quad (1)$$

where C_0 is the initial concentration of dye, and C is the concentration of dye after irradiation in selected time

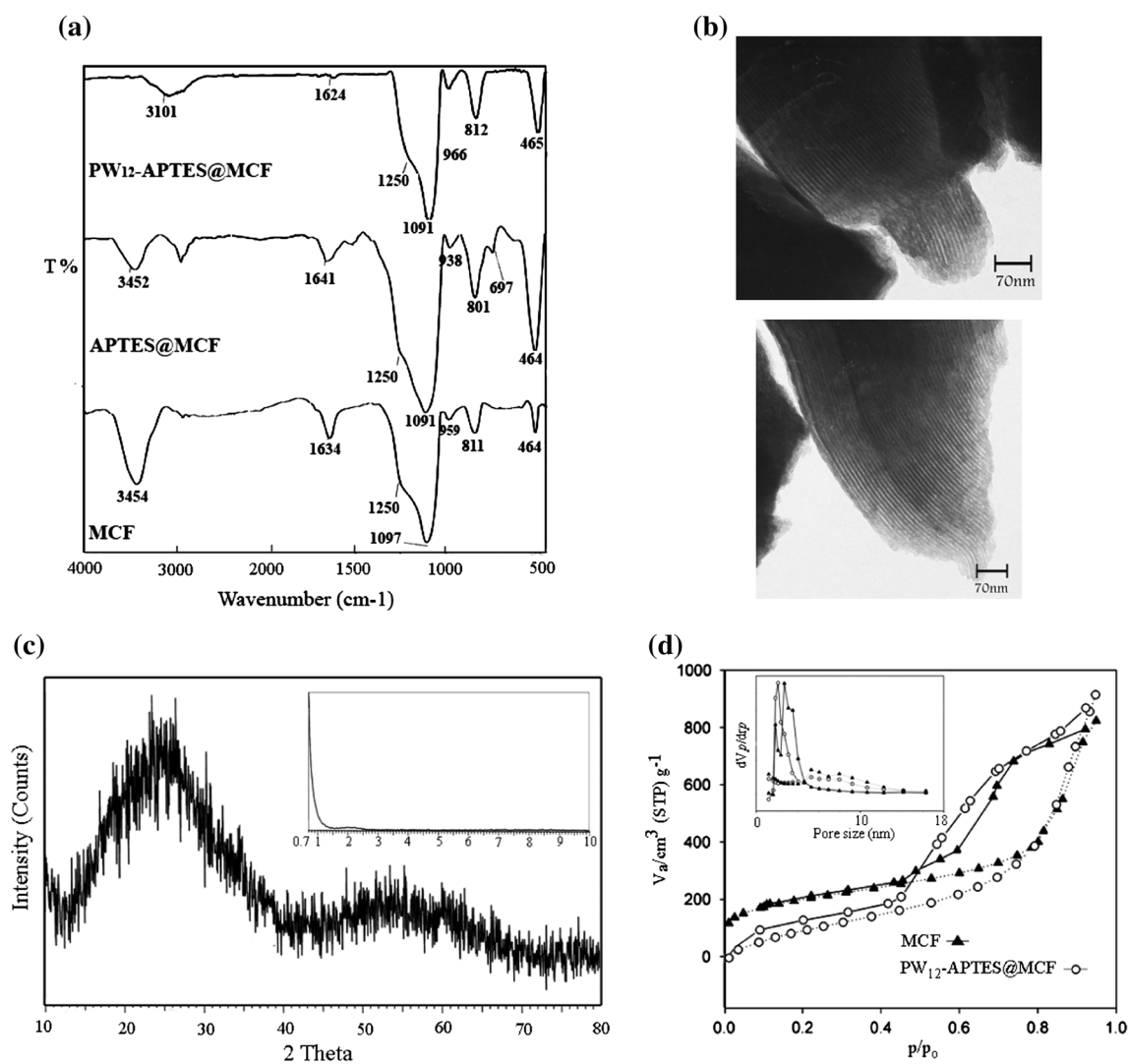


Fig. 1 **a** FTIR spectra of MCF materials, **b** TEM images and **c** XRD patterns ($2\theta = 10^\circ\text{--}80^\circ$) of $\text{PW}_{12}\text{-APTES@MCF}$, (inset: $2\theta = 0.7\text{--}10$); **d** N_2 adsorption–desorption isotherms and pore size distributions (inset) calculated by the BJH method of bare MCF and $\text{PW}_{12}\text{-APTES@MCF}$

Table 2 The texture parameters of parent silicas (MCF) and $\text{PW}_{12}\text{-APTES@MCF}$ in comparison with the bulk PW_{12} , $\text{PW}_{12}\text{-APTES@SBA-15}$ and $\text{PW}_{12}\text{-APTES@KIT-6}$

Entry	Sample	BET, surface area (m^2/g)	Pore volume (cm^3/g)	Pore diameter (nm)
1	MCF, silica	720	1.3	7.1
2	PW_{12}	6.0	–	–
3	$\text{PW}_{12}\text{-APTES@MCF}$	53	0.88	5.0
4	$\text{PW}_{12}\text{-APTES@SBA-15}$	75	0.91	5.1
5	$\text{PW}_{12}\text{-APTES@KIT-6}$	212	0.93	5.9

interval. In order to obtain maximum decolorization efficiency, the effects of key operating parameters such as dosage of photocatalyst, initial concentration of dye and solution pH (3–11) on photodecolorization process, were

Table 3 Photolytic and catalytic degradation of dyes after 30 min

Dye	Photolytic yield (%)	Catalytic yield (%)	Photocatalytic yield (%)
Roz.B	9.0	5.2	92
MG	7.0	5.0	93
3-BL	4.0	6.2	95
RhB	6.0	3.2	96
CI-50	3.0	2.2	90
MB	5.0	4.2	86

Reaction condition: dye (50 ppm), $\text{PW}_{12}\text{-APTES@MCF}$ (0.01 g), $V = 20$ mL

studied. To investigate the extent of surface adsorption during the decolorization of dye, control experiments in dark condition were performed at the presence of catalysts, in accordance to each case.

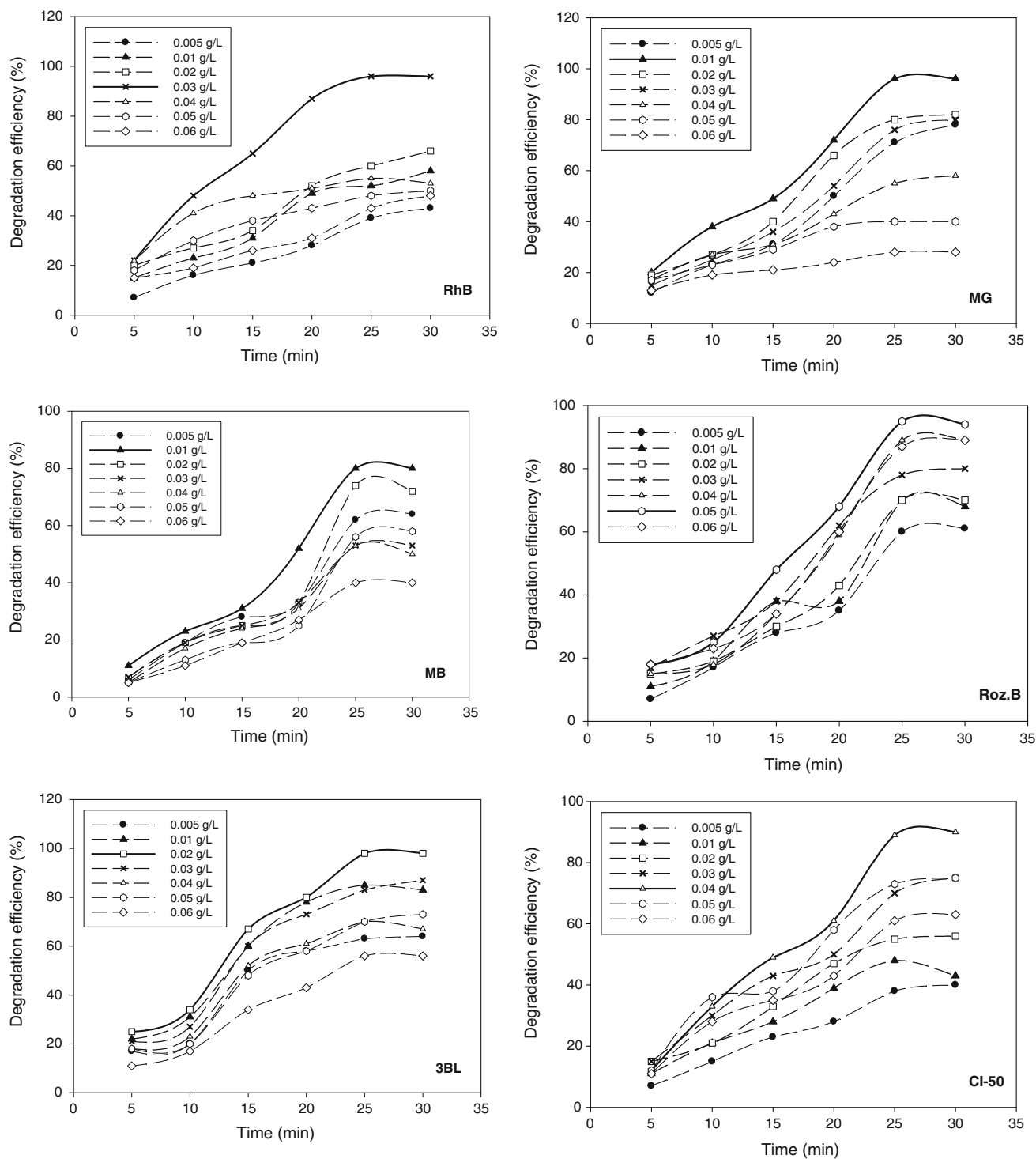


Fig. 2 Effect of catalysts dosage on the degradation efficiency. Initial dye concentration, 30 mg L^{-1} ; initial pH 7

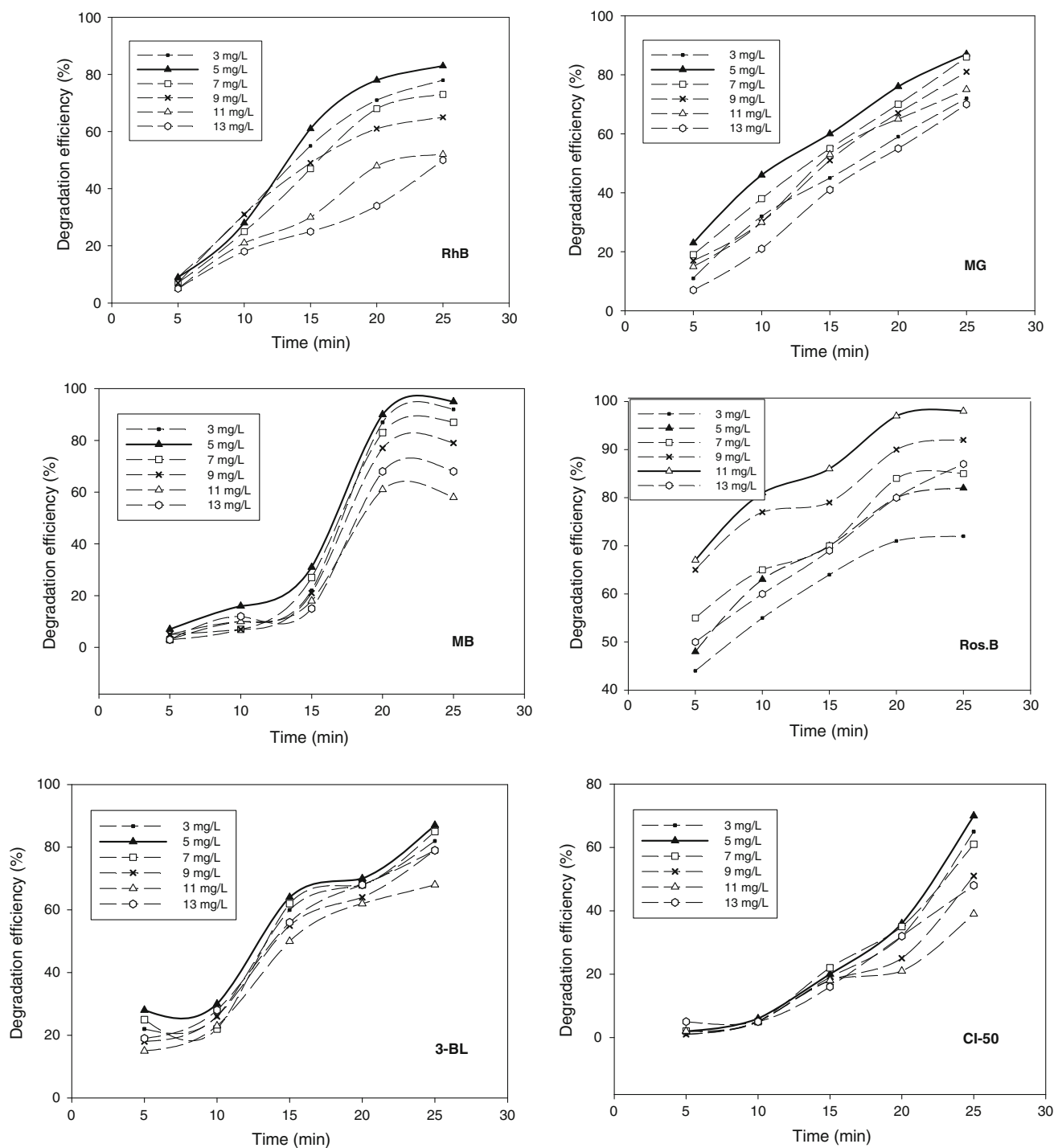


Fig. 3 Effect of initial dye concentration on the degradation efficiency of dyes; 30 g L^{-1} of the catalyst; initial solution pH 7

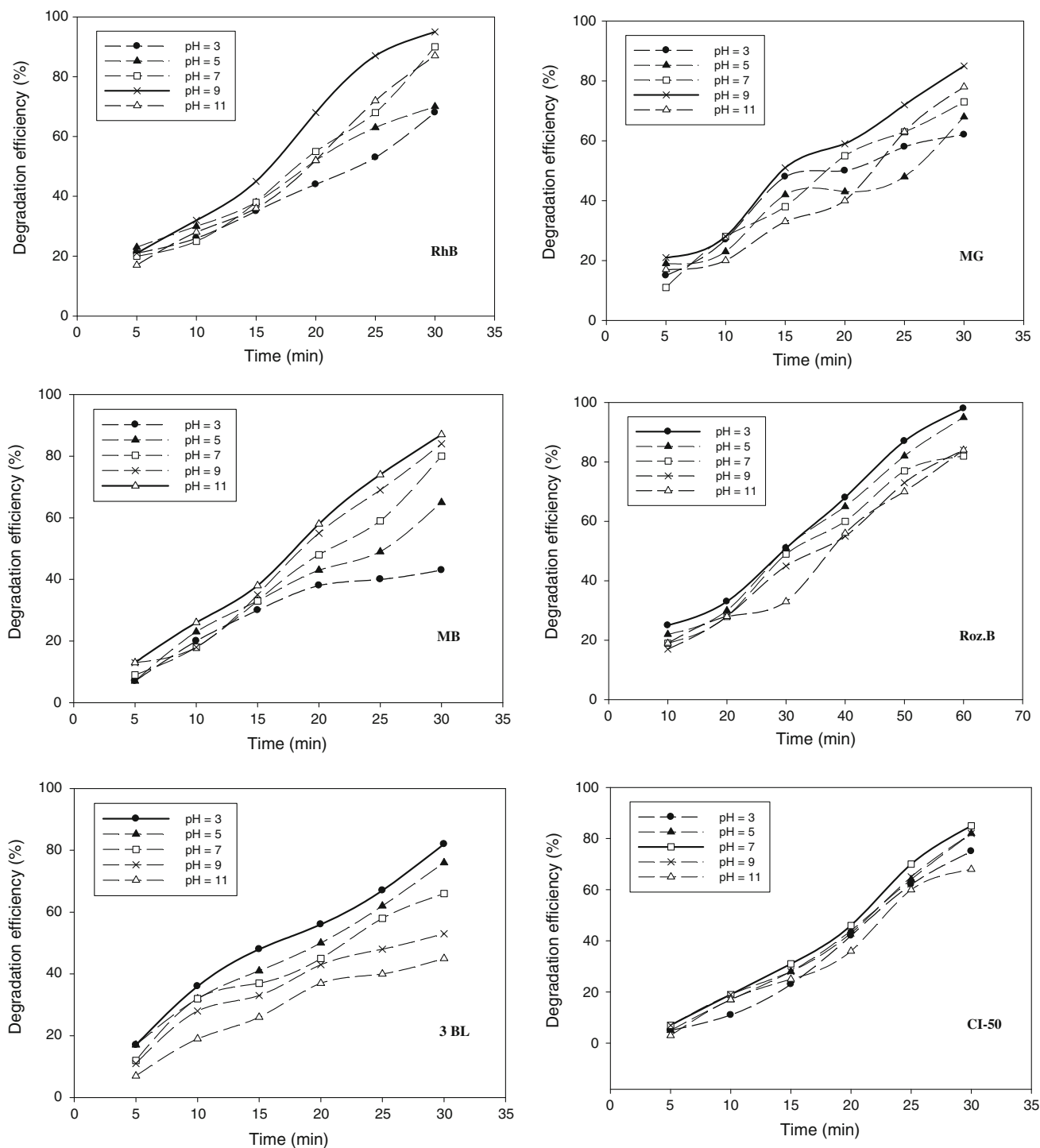


Fig. 4 Effect of solution pH on the degradation efficiency of dyes; 30 g L⁻¹ of the catalyst; initial dye concentration, 5 mg L⁻¹

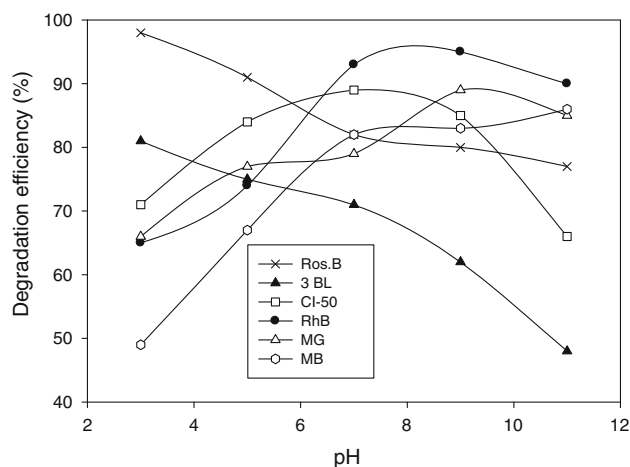


Fig. 5 Comparison of optimum pH of six dyes in photodegradation reaction in the presence of PW_{12} -APTES@MCF as photocatalyst

Results and discussion

Structural characterization

FTIR

Figure 1a presents the FTIR spectra in the skeletal region of $4,000\text{--}400\text{ cm}^{-1}$ for the MCF. A band at $1,624\text{--}1,641\text{ cm}^{-1}$ observed in all samples can be assigned to the $-\text{OH}$ vibration of physisorbed H_2O . In the case of unmodified MCF, the Si-O-Si bands originated from silica were observed at around $1,000\text{--}1,250$, $805\text{--}820$, and $461\text{--}475\text{ cm}^{-1}$. The amino functionalization followed by succinylation of the APTES@MCF was analyzed by FTIR spectroscopy. The broadband at $3,600\text{--}3,000\text{ cm}^{-1}$ for hydrogen bonded silanol [35, 36] was appreciably reduced in the modified samples. The organosilane presence was identified by the absorbance of the band $2,950\text{--}2,850\text{ cm}^{-1}$ for the propyl chain [37] and the deformation bands at $1,455\text{--}1,410\text{ cm}^{-1}$ [36]. The N-H absorption band overlapped with O-H bands at $3,300\text{--}3,500\text{ cm}^{-1}$ [26]. The presence of bands at $1,710\text{ cm}^{-1}$ (C=O , acid), $1,695\text{--}1,650\text{ cm}^{-1}$ (C=O amide I band), $1,566\text{--}1,561\text{ cm}^{-1}$ (NH amide II band) and $1,415\text{--}1,419\text{ cm}^{-1}$ ($-\text{C-N}$ amide) confirmed that succinylation had taken place [38]. The successful immobilization of the PW_{12} catalyst on the aminopropyl-functionalized MCF was confirmed by FTIR analyses as shown in Fig. 1. The primary structure of unsupported PW_{12} can be identified by the four characteristic IR bands appearing at $1,080\text{ cm}^{-1}$ (P-O band), 990 cm^{-1} (W=O band), 890 and 810 cm^{-1} (W-O-W bands) [39]. The characteristic IR bands of PW_{12} in the PW_{12} /APTES@MCF were different from those of unsupported PW_{12} . The P-O band in the PW_{12} /APTES@MCF was not clearly identified due to overlap by the broad

Si-O-Si band. However, W=O and W-O-W bands of PW_{12} in the PW_{12} -APTES@MCF appeared at slightly shifted positions compared to those of the unsupported PW_{12} , indicating a strong interaction between PW_{12} and APTES@MCF [34].

TEM

Figure 1b shows the TEM images of PW_{12} -APTES@MCF. The places with darker contrast could be assigned in the presence of PW_{12} particles with different dispersion. The small dark spots in the images could be ascribed to PW_{12} particles, probably located into the support channels. The larger dark areas over the channels most likely correspond to PW_{12} agglomerates on the external surface [40, 41].

XRD

Figure 1c shows the XRD patterns of PW_{12} -APTES@MCF in ($2\theta = 10^\circ\text{--}80^\circ$). What is interesting is that all samples showed no characteristic XRD pattern, even though 35 % wt% PW_{12} was loaded on the mesoporous silicas. This indicates that the PW_{12} species were not in a crystal state but in an amorphous-like state, demonstrating that Keggin species are finely and molecularly dispersed on the mesoporous silicas. Figure 1c (inset) shows the XRD patterns of the modified MCF within the 2θ range of $0.7^\circ\text{--}10^\circ$. There was no significant peak observed for PW_{12} /APTES@MCF [42].

N_2 adsorption–desorption isotherms

Figure 1d shows the N_2 adsorption–desorption isotherms and pore size distributions of unmodified MCF and PW_{12} -APTES@MCF. All the samples exhibited typical IV type isotherms and H1 type hysteresis loops at high relative pressures according to the IUPAC nomenclature [43], which are the typical characteristics of mesoporous materials [44–46]. Physical properties of unmodified MCF, PW_{12} (bulk) and modified silicas (PW_{12} -APTES@MCF, PW_{12} -APTES@SBA-15 and PW_{12} -APTES@KIT-6) are listed in Table 2. PW_{12} -APTES@MCF has the lowest surface area in these series. As expected, the BET surface areas and total pore volumes of unmodified MCF are decreased after the functionalization with PW_{12} . These changes reflect that part of the mesopore volumes in the silica matrixes is filled with PW_{12} . In addition, the pore size distribution of unmodified MCF and PW_{12} -APTES@MCF was calculated using the Barrett–Joyner–Halenda (BJH) model on the adsorption branch of the N_2 adsorption/desorption isotherm. Figure 1d (inset) shows that the pore size distribution of PW_{12} -APTES@MCF is narrow, in the range of 2–7 nm (centered at 4.4 nm).

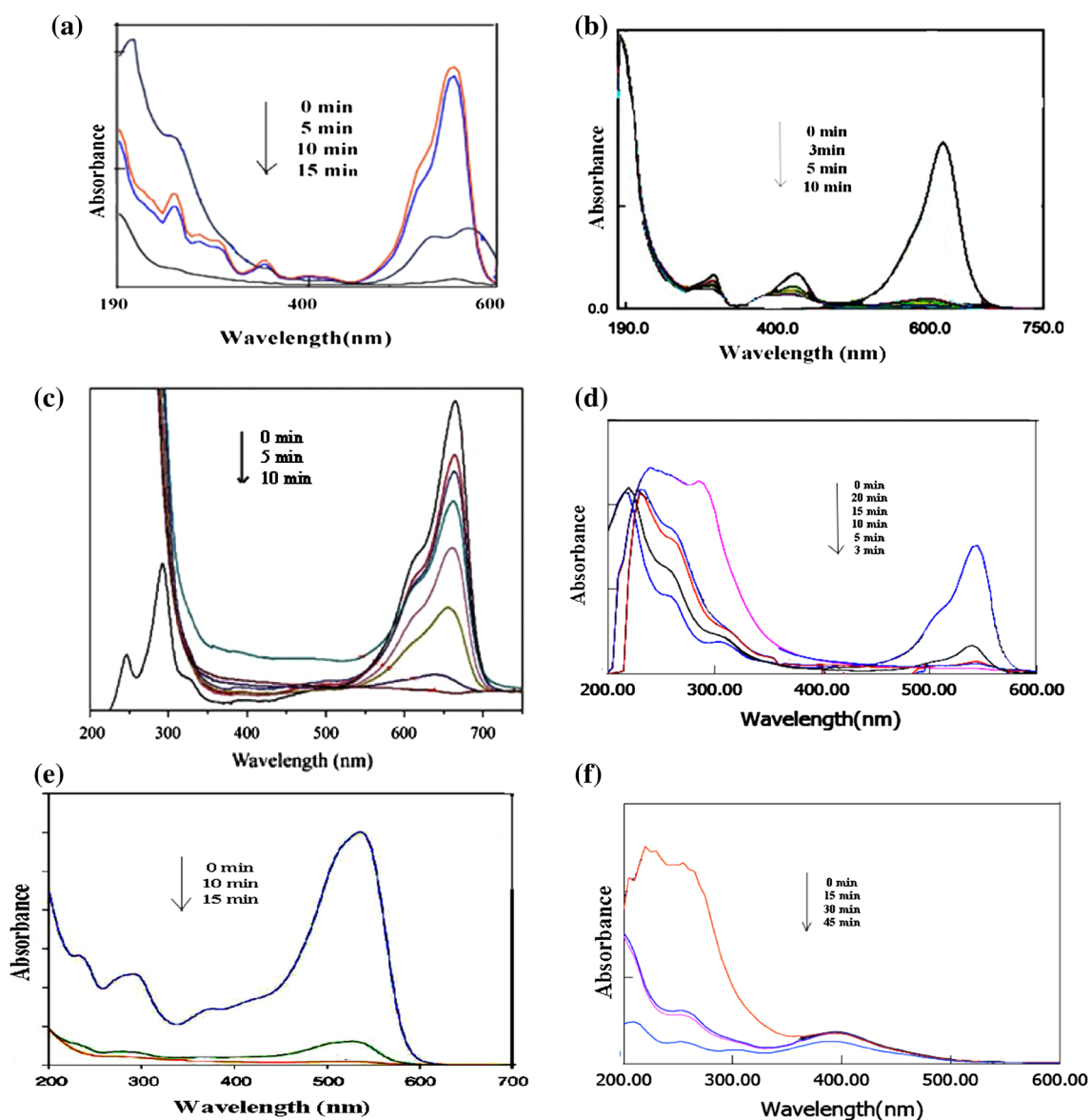


Fig. 6 Change in absorbance spectra of dye with the illumination time for the PW_{12} -APTES@MCF photocatalyst: **a** RhB (photocatalyst 30 g L^{-1} , dye concentration 5 mg L^{-1} and pH 9), **b** MG (photocatalyst 10 g L^{-1} , dye concentration 5 mg L^{-1} and pH 9), **c** MB (photocatalyst 10 g L^{-1} , dye concentration 5 mg L^{-1} and pH

11), **d** Roz.B (photocatalyst 50 g L^{-1} , dye concentration 11 mg L^{-1} and pH 3), **e** 3-BL (photocatalyst 20 g L^{-1} , dye concentration 5 mg L^{-1} and pH 3), and **f** CI-50 (photocatalyst 40 g L^{-1} , dye concentration 5 mg L^{-1} and pH 7)

Photocatalytic tests

Blank experiments

To estimate the contribution of direct ‘photolysis’ to the overall photodegradation of dyes, the photodegradation of pure dyes was measured. For this purpose, a tank of pure dye (blank) under similar conditions was put beside every tank containing suspension. To determine the surface adsorption amount, controlled experiments in the dark condition were carried out at the presence of the catalyst. In the absence of catalyst, direct photolysis of dyes was very slow and no

Table 4 Optimum irradiation time for the photodegradation of dyes in the presence of PW_{12} -APTES@MCF photocatalyst at the optimum conditions

Dye	RhB	MG	MB	Roz.B	3-BL	CI-50
Optimum irradiation time (min)	15	5	10	3	15	45

appreciable photodegradation, about 3–9 % was observed during 30 min of UV irradiation (Table 3, entry 2), while in the presence of catalyst, the percent of dye which is degraded

Table 5 Comparison of kinetics of dyes' decolorization of PW₁₂-APTES@MCF with two other PW₁₂-APTES@silica (SBA-15 and KIT-6) at the maintained optimum conditions for each dye (photocatalyst, dye concentration and pH)

Photocatalyst	Decolorization (%)	Rate constant ($k \times 10^3 \text{ min}^{-1}$)
(a) Rhodamine B (after 15-min irradiation)		
PW ₁₂ -APTES@MCF	96.8	82.0
PW ₁₂ -APTES@SBA-15	95.6	76.0
PW ₁₂ -APTES@KIT-6	95.3	74.0
(b) Malachite green (after 5-min irradiation)		
PW ₁₂ -APTES@MCF	96.5	242
PW ₁₂ -APTES@SBA-15	93.1	196
PW ₁₂ -APTES@KIT-6	89.0	157
(c) Methylene blue (after 10-min irradiation)		
PW ₁₂ -APTES@MCF	86.2	68.0
PW ₁₂ -APTES@SBA-15	84.3	62.0
PW ₁₂ -APTES@KIT-6	79.8	47.0
(d) Rose bengal (after 3-min irradiation)		
PW ₁₂ -APTES@MCF	98.9	500
PW ₁₂ -APTES@SBA-15	92.8	320
PW ₁₂ -APTES@KIT-6	87.3	240
(e) Solophenyl red (after 15-min irradiation)		
PW ₁₂ -APTES@MCF	98.1	92.0
PW ₁₂ -APTES@SBA-15	97.0	84.0
PW ₁₂ -APTES@KIT-6	86.6	46.0
(d) Yellow direct 50 (after 45-min irradiation)		
PW ₁₂ -APTES@MCF	98.0	30.0
PW ₁₂ -APTES@SBA-15	89.0	17.0
PW ₁₂ -APTES@KIT-6	85.0	14.0

after 30 min ranged from 3–9 % to 86–96 % (Table 3, entry 4). The results also showed that PW₁₂-APTES@MCF catalysts alone did not result in any significant degradation of the mentioned dyes (Table 3, entry 3).

Effect of photocatalyst dosage

The effect of the amount of PW₁₂-APTES@MCF on the photodegradation of dye versus time is shown in Fig. 2. It was observed that the degradation percentage increased with increasing the mass of photocatalyst and then decreased. The enhancement of photodegradation efficiency of the dyes with increasing the mass of photocatalyst may be attributed to the rapid transfer of the photo-generated electrons resulting in the effective separation of the electrons and holes [47]. Hole can oxidize the H₂O that is adsorbed on the MCF surface, to form the free radical of ·OH. The radical of ·OH combined on MCF surface is a strong oxidant and oxidizes the adjacent organic compound. In order to shed some light on the role of hydroxyl radicals (·OH) as a major active species during the photocatalytic

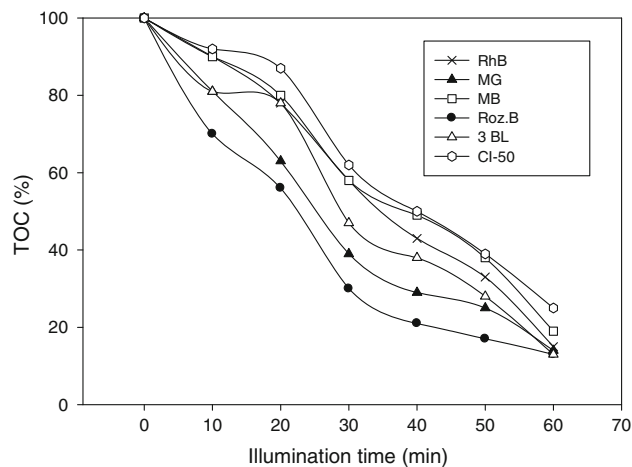


Fig. 7 Decrease in TOC of six dye aqueous solutions in the presence of PW₁₂-APTES@MCF during illumination

Table 6 Investigation of the feasibility of reusing of PW₁₂-APTES@MCF in the photodegradation of Roz.B dye (as model)

Run	Degradation (%)	Amount of W leached (%) ^a
1	95.78	–
2	94.3	–
3	93.9	–
4	88.4	0.02
5	86.3	0.07

^a Determined by NAA

oxidation reaction, (2,2,6,6-tetramethylpiperidin-1-yl)oxyl (TEMPO) was used as a scavenger of ·OH. Notably, with the addition of TEMPO to remove the ·OH, the photodegradation efficiency of MG has no significant change, indicating that the ·OH in the solution bulk is not a major reactive species.

The reason for this decrease is thought to be the fact that when the concentration of the catalyst rises, the solid particles increasingly block the penetration of the photons. Hence, the overall number of the photons that reach the catalyst particles and the production of OH radicals decrease [48]. Another reason may be due to the aggregation of solid particles when a large amount of catalyst is used [49]. It is clear that at high concentration of catalyst, the degradation rate decreases due to the reduction of the photonic flux within the irradiated solution.

Effect of initial dye concentration

The effect of initial dye concentration (Fig. 3) ranging from 3 to 13 ppm on photodegradation of dyes by photocatalyst was investigated under UV irradiation. The obtained results as a function of the initial dye concentration on the dye photodegradation efficiency are presented

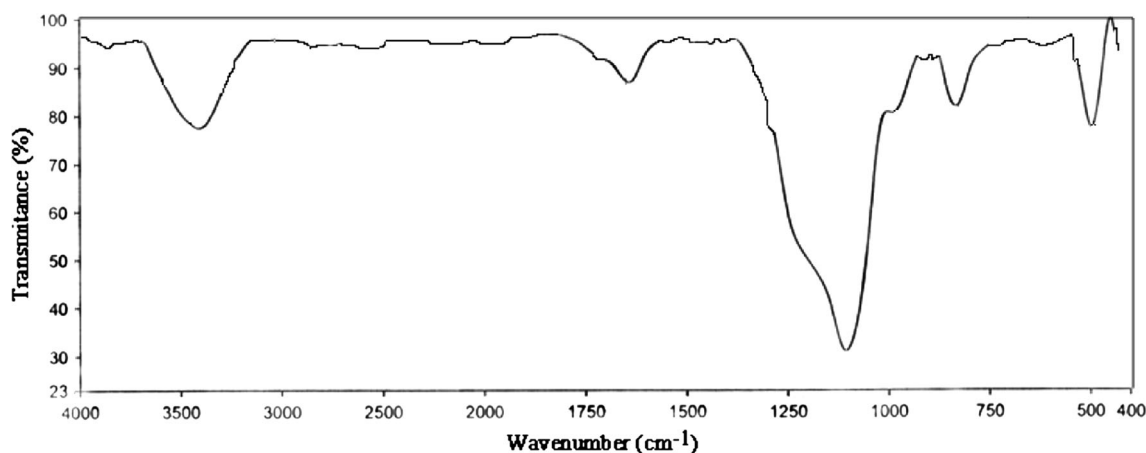


Fig. 8 a FTIR spectra of the recovered PW_{12} -APTES@MCF in the photodegradation of Roz.B (as model dye)

in Fig. 3. It can be seen that the photodegradation efficiency of dye decreased with increasing initial concentration of dye from optimum values. One possible cause for such results is the UV radiation-screening effect of the dye itself. At a high dye concentration, a significant amount of UV radiation may be absorbed by the dye molecules rather than the catalyst particles. Consequently, by increasing the initial dye concentration, the photon flow reaching the catalyst particles decreased due to the fact that increasing numbers of photons were absorbed by the dye molecules present in the solution and/or on the catalyst surface, thus reducing the efficiency of the catalytic reaction [50]. Another possible cause is the interference from intermediates formed upon UV photocatalytic of the parental dye. These intermediates may include aromatics, aldehydes, ketones and organic acids as shown by previous studies with various aromatic compounds [51–53]. They may compete with the dye molecules for the limited adsorption and catalytic sites on the catalyst particles, and thus inhibit decolorization.

Effect of pH

The most important parameter that influences the photocatalytic degradation is solution pH. The effect of pH value was also studied (Figs. 4, 5) by adding incremental amounts of either concentrated HCl or NaOH to the dye solution in the presence of UV/ PW_{12} -APTES@MCF.

The effect of pH value (Fig. 4) on the degradation efficiency of dye in the range of 3–11 was further investigated. Figure 5 shows the % change in degradation of the dye at five different pH values for 6 dyes. The cationic dyes (such as RhB, MG and MB) underwent efficient degradation in the presence of PW_{12} -APTES@MCF under UV-Vis irradiation in alkaline media. Anionic dyes (such as Roz.B, 3BL and CI-50) exhibited rather slow photoreaction under

the same conditions in alkaline media. These observations suggest that the charge characteristics of the dye substrates greatly influence their degradation. The effect of pH on the degradation of dyes in the presence of SiO_2 has been explained on the basis of point of zero charge (pH_{pzc}) of SiO_2 particles. The pH_{pzc} of SiO_2 particles is 5.5 [54]. Thus, SiO_2 is positively charged in acidic solution ($pH < 5.5$) and negatively charged in alkaline solution. According to this explanation and because of electrostatic interactions, cationic dyes (Rh.B, MG and MB, optimum pH: 9, 9 and 11, respectively) should be degraded at alkaline solution, and anionic dyes (Roz.B and 3BL, optimum pH: 3) should be degraded effectively in acidic solutions (Fig. 5). In alkaline solutions, interaction between catalyst surface ($Si-O^-$) and dye [specifically the nitrogen group, such as RhB, MG, MB, (Fig. 1)] favors the adsorption of the dye on the surface and accordingly the photocatalytic activity increases [55]. The results showed that negatively charged dyes are degraded efficiently at acidic solutions (Figs. 4, 5).

UV-Vis studies

Figure 6 shows photodegradation of dyes under irradiation time and in the presence of PW_{12} -APTES@MCF photocatalyst at the optimum conditions (photocatalyst, dye concentration and pH). The decrease of samples absorbance due to the decrease of dye concentration was recorded for the measurement of photodegradation rate in all above-mentioned parameters. Since there were no additional peaks appearing in the UV-Vis spectra, the dye was completely degraded. After being irradiated under UV light for 2 min to Roz.B dye, the degradation efficiency was 72.34 % and it reached 95.78 % after 3 min. For other dyes, optimum irradiation time was listed in Table 4. Maximum irradiation time is 45 min for CI-50.

Photodegradation rate constants

The photocatalytic activity of three different photocatalysts including PW₁₂-APTES@MCF, PW₁₂-APTES@SBA-15 and PW₁₂-APTES@KIT-6 with the same mole was compared through the degradation of mentioned dyes under UV–Vis irradiation (Table 5). From the results shown in Table 5, it is found that the PW₁₂-APTES@KIT-6 is less photoactive than the corresponding modified SBA-15, but the PW₁₂-APTES@MCF is more photoactive than PW₁₂-APTES@SBA-15. For example, after 3 min UV–Vis irradiation, Roz.B is almost completely degraded by the PW₁₂-APTES@MCF; however, Roz.B remains 7.2 and 12.7 %, respectively, in the PW₁₂-APTES@SBA-15 and PW₁₂-APTES@MCF photocatalyzed reaction systems. Moreover, from the observed activity order for degradation, we see that the photocatalytic activities of the porous composites were independent on their BET surface areas (Table 2).

In order to calculate photodegradation rate constants, k values, $\ln(C^0/C)$ is plotted as a function of the irradiation time. The rate constant values, $k \times 10^3$ (min⁻¹), are calculated from the slopes of the straight-line portion of the first-order plots as a function of the catalyst mass and are listed in Table 5.

To confirm of complete degradation of dyes, photodegradation of six dyes was evaluated in the presence of PW₁₂-APTES@MCF by monitoring the reaction of total organic carbon (TOC) with a TOC analyzer, and the degradation measurement was obtained from the normalized equation: % TOC = $(\text{TOC}_{\text{initial}} - \text{TOC}_{\text{final}}) / \text{TOC}_{\text{initial}} \times 100$. %TOC reduction of dye solutions is shown in Fig. 7, which shows that degradation of dyes is almost complete. In the presence investigation, TOC has a rapid decrease to 91 % within 60 min for Roz.B degradation in the presence of PW₁₂-APTES@MCF and no considerable change was observed after it, which indicates the formation of intermediates that are resistant to further degradation. The results have shown that minimum TOC removal (80 %) within 60 min for CI-50 degradation in the presence of PW₁₂-APTES@MCF has the slowest decrease in these series, clearly indicating that the PW₁₂-APTES@MCF has the minimum photocatalytic activity for CI-50 degradation. The results (Fig. 7) also show that, loss of the CI-50 active groups is hardest rather than other mentioned dyes during the degradation processes.

Reusability

PW₁₂-APTES@MCF was reused several times to determine whether the photocatalyst suffered from permanent deactivation. The wet catalyst was recycled [the nature of the recovered catalysts has been followed by neutron

activation analysis (NAA), (Table 6) and FTIR spectra (Fig. 8)], and no appreciable change in activity was noticed after three cycles (Table 6). The FTIR spectra of the recovered PW₁₂-APTES@MCF (Fig. 8) are as same as the fresh catalyst.

Conclusions

The results of this research demonstrated that PW₁₂-APTES@MCF affects the catalyst during the photodegradation of RhB, MG, MB, Roz.B, 3-BL and CI-50. The results of UV–Vis spectra changes and TOC decrease indicate that photocatalytic process can be used for complete degradation and mineralization of the six mentioned dye pollutants in the presence of PW₁₂-APTES@MCF in a photochemical reactor. PW₁₂-APTES@MCF shows high photocatalytic activity, and maximum degradation takes place for Roz.B at optimum conditions.

Acknowledgments We gratefully thank Shahreza Branch, Islamic Azad University, for financial support.

References

1. C. Galindo, P. Jacques, A. Dalt, *Chemosphere* **45**, 997 (2001)
2. J.M. Herrmann, M. Vautier, C. Guillard, *J. Catal.* **201**, 46 (2001)
3. U. Pagga, K. Taeger, *Water Res.* **28**, 1051 (1994)
4. M.R. Hoffmann, S.T. Martin, W. Choi, D.W. Bahnemann, *Chem. Rev.* **95**, 69 (1995)
5. B. Neppolian, S. Sakthivel, M. Palanichamy, B. Arabindoo, V. Murugasan, *Stud. Surf. Sci. Catal.* **113**, 329 (1998)
6. J. Guo, Y. Li, S. Zhu, Z. Chen, Q. Liu, D. Zhang, W.-J. Moon, D.-M. Song, *RSC Adv.* **2**, 1356 (2012)
7. R. Dillert, D. Bahnemann, H. Hidaka, *Chemosphere* **67**, 785 (2007)
8. K.Y. Ho, G. McKay, K.L. Yeung, *Langmuir* **19**, 3019 (2003)
9. R.K. Dey, F.J.V.E. Oliveira, C. Airoidi, *Colloid Surf. A* **324**, 41 (2008)
10. X. Feng, G.E. Fryxell, L.O. Wang, A.Y. Kim, J. Liu, K.M. Kemner, *Science* **276**, 923 (1997)
11. M.H. Lim, A. Stein, *Chem. Mater.* **11**, 3285 (1999)
12. A. Pearson, S.K. Bhargava, V. Bansal, *Langmuir* **27**, 9245 (2011)
13. C. Yang, L.T. Changjun, L. Ye, T. Peng, K. Deng, L. Zan, *J. Appl. Polym. Sci.* **120**, 2048 (2011)
14. Z. Jiang, J. Han, X. Liu, *Adv. Mater. Res.* **152–153**, 202 (2011)
15. Y.W. Chang, N.J. Kim, C.S. Lee, *Adv. Mater. Proc.* **26–28**, 1083 (2007)
16. C. Chen, Q. Wang, P. Lei, W. Song, W. Ma, J. Zhao, *Environ. Sci. Technol.* **40**, 3965 (2006)
17. K. Lv, Y. Xu, *J. Phys. Chem. B* **110**, 6204 (2006)
18. H. Einaga, M. Misono, *Bull. Chem. Soc. Jpn* **69**, 3435 (1996)
19. A. Mylonas, A. Hiskia, E. Papaconstantinou, *J. Mol. Catal. A Chem.* **114**, 191 (1996)
20. A. Molinari, R. Amadelli, V. Carassiti, A. Maldotti, *Eur. J. Inorg. Chem.* **91** (2000)
21. D.A. Friesen, L. Morello, J.V. Heaaley, C.H. Langford, *J. Photochem. Photobiol. A Chem.* **133**, 213 (2000)
22. R.D. Gall, C.L. Hill, J.E. Walker, *Chem. Mater.* **8**, 2523 (1996)

23. N. Mizuno, M. Misono, Chem. Rev. **98**, 199 (1998)
24. L.K. Kolkova, E.S. Rudakov, V.P. Tretyakov, Kinet. Katal. **37**, 540 (1996)
25. Y. Guo, Y. Wang, C. Hu, E. Wang, Chem. Mater. **12**, 3501 (2000)
26. Y. Guo, D. Li, C. Hu, Y. Wang, E. Wang, Y. Zhou, S. Feng, Appl. Catal. B Environ. **30**, 337 (2001)
27. R. Fazaeli, S. Tangestaninejad, H. Aliyan, Appl. Catal. A **318**, 218 (2007)
28. R. Fazaeli, H. Aliyan, Appl. Catal. A Gen. **331**, 78 (2007)
29. R. Fazaeli, H. Aliyan, Appl. Catal. A Gen. **353**, 74 (2009)
30. A. Nezamzadeh-Ejehieh, S. Hushmandrad, Appl. Catal. A Gen. **388**, 149 (2010)
31. H. Salavati, N. Tavakkoli, M. Hosseinpour, Ultrason. Sonochem. **19**, 546 (2012)
32. L. You-ji, C. Wei, Catal. Sci. Technol. **1**, 802 (2011)
33. P. Schmidt-Winkel Jr., W.W. Lukens, P. Yang, D.I. Margolese, J.S. Lettow, J.Y. Ying, G.D. Stuck, Chem Mater. **12**, 686 (2000)
34. V.D. Chaube, S. Shylesh, A.P. Singh, J. Mol. Catal. A Chem. **241**, 79 (2005)
35. I. Diaz, C. Marquez-Alvarez, F. Mahino, J. Perez-Periente, E. Sastre, J. Catal. **193**, 283 (2000)
36. B.H. Wouters, T. Chen, M. Dewilde, P.J. Grobet, Micropor. Mesopor. Mater. **44–45**, 453 (2001)
37. A.B. Jarzębski, K. Szymańska, J. Bryjak, J. Mrowiec-Białoń, Catal. Today **124**, 2 (2007)
38. J. Aburto, M. Ayala, I. Bustos-Jaimes, C. Montiel, E. Terrés, J.M. Domínguez, E. Torres, Micropor. Mesopor. Mater. **83**, 193 (2005)
39. I.V. Kozhevnikov, *Catalysis by Polyoxometalates* (Wiley, England, 2002)
40. T. Tsoncheva, L. Ivanova, J. Rosenholm, M. Linden, Appl. Catal. B Environ. **89**, 365 (2009)
41. D.G. Castner, PhR Watson, I.Y. Chan, J. Phys. Chem. **93**, 3188 (1989)
42. K. Kannan, R.V. Jasra, J. Mol. Catal. B Enzym. **56**, 34 (2009)
43. K.S.W. Sing, D.H. Everett, R.A.W. Haul, L. Moscou, R.A. Pierotti, J. Rouquerol, Pure Appl. Chem. **57**, 603 (1985)
44. J.S. Beck, J.C. Vartuli, W.J. Roth, M.E. Leonowicz, C.T. Kresge, K.D. Schmitt, J. Am. Chem. Soc. **114**, 10834 (1992)
45. C.T. Kresge, M.E. Leonowicz, W.J. Roth, J.C. Vartuli, J.S. Beck, Nature **359**, 710 (1992)
46. M. Che, J.C. Védrine, *Characterization of Solid Materials and Heterogeneous Catalysts: From Structure to Surface Reactivity* (Wiley-VCH, New York, 2012), pp. 853–879
47. U. Stafford, K.A. Gray, P.V. Kamat, J. Catal. **167**, 25 (1997)
48. M.B. Kasiri, H. Aleboeyeh, A. Aleboeyeh, Appl. Catal. B Environ. **84**, 9 (2008)
49. Z.M. El-Bahy, M.M. Mohamed, F.I. Zidan, M.S. Thabet, J. Hazard. Mater. **153**, 364 (2008)
50. A. Mills, R.H. Davis, D. Worsley, Chem. Soc. Rev. **22**, 417 (1993)
51. N. Serpone, R. Terzian, C. Minero, E. Pelizzetti, *Photosensitive Metal-Organic Systems: Mechanistic Principles and Applications* (American Chemical Society, Washington D.C., 1993), p. 281
52. O. d’Henezel, P. Pichat, D.F. Ollis, J. Photochem. Photobiol. A Chem. **118**, 197 (1998)
53. K. Tanaka, K. Padermpole, T. Hisanaga, Water Res. **34**, 327 (2000)
54. E. Ordóñez Regil, E. Ordóñez Regil, N. García González, S.R. Barocio, Am. J. Anal. Chem. **3**, 512 (2012)
55. M.B. Kasiri, H. Aleboeyeh, A. Aleboeyeh, Appl. Catal. B Environ. **84**, 9 (2008)